

Nucleon charge and magnetisation distributions: flavour separation and zeroes

Zhao-Qian Yao (姚照千)^{ID,a,b,c}, Daniele Binosi^{ID,c}, Zhu-Fang Cui (崔著钊)^{ID,a,b}, Craig D. Roberts^{ID,*a,b}

^a School of Physics, Nanjing University, Nanjing, Jiangsu 210093, China

^b Institute for Nonperturbative Physics, Nanjing University, Nanjing, Jiangsu 210093, China

^c European Centre for Theoretical Studies in Nuclear Physics and Related Areas (ECT*), Villa Tambosi, Strada delle Tabarelle 286, I-38123 Villazzano (TN), Italy
zyao@ectstar.eu (ZQY); binosi@ectstar.eu (DB); phycui@nju.edu.cn (ZFC); cdroberts@nju.edu.cn (CDR)

Date: 2024 November 06

Abstract

A symmetry-preserving truncation of the quantum field equations describing hadron properties is used to deliver parameter-free predictions for all nucleon elastic electromagnetic form factors and their flavour separation to large values of momentum transfer, Q^2 . The proton electric form factor, G_E^p , possesses a zero, whereas that of the neutron, G_E^n , does not. The difference owes to the behaviour of the Pauli form factor of the proton's singly-represented valence d -quark. Consequently, $G_E^n > G_E^p$ on a material large- Q^2 domain. These predictions can be tested in modern experiments.

Keywords: continuum Schwinger function methods, Dyson-Schwinger equations, elastic electromagnetic form factors, emergence of mass, nucleons - neutrons and protons, nonperturbative quantum field theory, quantum chromodynamics

1. Introduction

The proton is Nature's most fundamental bound state. It is supposed to be explained by quantum chromodynamics (QCD), the Poincaré-invariant quantum non-Abelian gauge field theory that describes strong interactions in the Standard Model. The QCD Lagrangian density is expressed in terms of gluon and quark partons (and ghosts, too, in many gauges) [1]. In these terms, the proton consists of three valence-quark partons ($u + u + d$) and infinitely many gluon and sea-quark partons – see Fig. 1. If science is to claim an understanding of Nature, then it must deliver a sound description of proton properties from QCD; not just its mass, but also its entire array of structural properties [2–7].

The proton bound-state problem can be addressed in any approach that provides access to the three-quark six-point Schwinger function [8, 9]. Lattice-regularised QCD (lQCD) provides one such framework. Modern applications are sketched in Ref. [10, Sec. 10]. Continuum Schwinger function methods (CSMs) provide another widely used approach to nucleon (proton, p , and neutron, n) structure [11–15]. Many such studies use a quark + dynamical diquark picture of the nucleon because it vastly simplifies the problem [16]. Notwithstanding that, the approximations implicit in the simplification need checking and tighter links must be forged with QCD. These things can be accomplished by beginning with an explicitly symmetry-preserving truncation of all quantum field equations (Dyson-Schwinger equations – DSEs) relating to the nucleon bound-state problem. The first study of this type was reported in Ref. [17].

A highlight of proton structure studies this century is the collection of data that hints at the existence of a zero in the

proton elastic electric form factor [18–22]. (A zero in the transverse helicity amplitude associated with the proton \rightarrow Roper transition has unambiguously been located [12].) This is complemented by the discovery of marked differences in the charge and magnetisation distributions of different valence-quark flavours (u vs. d) within the proton [23, 24]. These features have attracted much attention [16, 25–29]. Modern and foreseen facilities will both obtain data that can check existing measurements and push empirical knowledge of all nucleon form factors to momentum transfers $Q^2 > 10 \text{ GeV}^2$ [24, 30]. This prospect challenges theory to deliver predictions for all such form factors that extend far onto this domain in frameworks with a traceable connection to QCD.

Herein, we approach this challenge by using the rainbow-ladder (RL) truncation of all DSEs needed to calculate the matrix element from which nucleon elastic electromagnetic form factors can be extracted. This is the leading-order in a symmetry-preserving, systematically-improvable scheme [31].

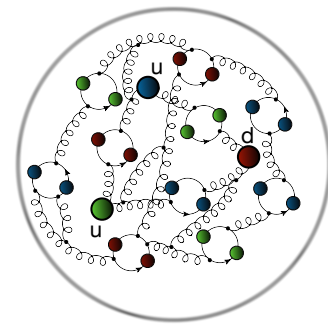


Figure 1: Proton: two valence up (u) quark partons, one valence down (d) quark parton, and infinitely many gluon and sea-quark partons, drawn here as “springs” and closed loops, respectively. The neutron is the proton's isospin partner, two d quark partons, one u quark parton, and gluon and sea.

*Corresponding author

[†]All authors contributed equally to this work.

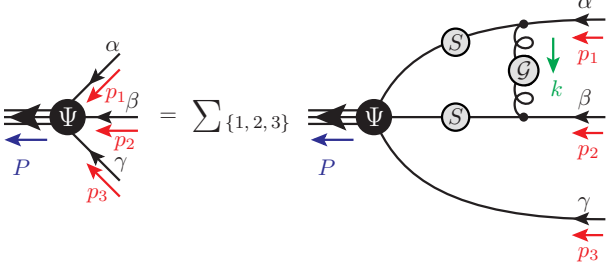


Figure 2: Faddeev equation. Filled circle: Faddeev amplitude, Ψ , the matrix-valued solution, which involves 128 independent scalar functions. Spring: dressed-gluon interaction that mediates quark+quark scattering, Eqs. (1), (2). Solid line: dressed-quark propagator, S , calculated from the rainbow gap equation. Lines not adorned with a shaded circle are amputated. Isospin symmetry is assumed.

Existing algorithms have limited the reach of such form factor calculations to $Q^2 \lesssim 4 \text{ GeV}^2$. We extend the results to $Q^2 \gtrsim 12 \text{ GeV}^2$ using the statistical Schlessinger point method (SPM) [32–34], which may also be called a statistical multi-point Padé approximant scheme. The SPM is grounded in analytic function theory. It is free from practitioner-induced bias; hence, delivers objective analytic continuations with quantitatively reliable uncertainties.

2. Methods and Tools

2.1. Nucleon Bound State

The RL truncation nucleon Faddeev equation is drawn in Fig. 2. Discussions of the formulation and solution of this linear, homogeneous integral equation are provided, *e.g.*, in Ref. [35, 36]. The key element is the quark + quark scattering kernel, for which the RL truncation is obtained by writing [37]:

$$\mathcal{K}_{tu}^{rs}(k) = \tilde{\mathcal{G}}(y)[i\gamma_\mu \frac{\lambda^a}{2}]_{ts}[i\gamma_\nu \frac{\lambda^a}{2}]_{ur}T_{\mu\nu}(k), \quad (1)$$

$k^2 T_{\mu\nu}(k) = k^2 \delta_{\mu\nu} - k_\mu k_\nu$, $y = k^2$. The tensor structure specifies Landau gauge, used because it is a fixed point of the renormalisation group and that gauge for which corrections to RL truncation are least significant [38]. In Eq. (1), r, s, t, u represent colour, spinor, and flavour matrix indices (as necessary).

A realistic form of $\tilde{\mathcal{G}}_{\mu\nu}(y)$ is explained in Refs. [41, 42]:

$$\tilde{\mathcal{G}}(y) = \frac{8\pi^2}{\omega^4} D e^{-y/\omega^2} + \frac{8\pi^2 \gamma_m \mathcal{F}(y)}{\ln[\tau + (1 + y/\Lambda_{\text{QCD}}^2)^2]}, \quad (2)$$

where $\gamma_m = 12/25$, $\Lambda_{\text{QCD}} = 0.234 \text{ GeV}$, $\tau = e^2 - 1$, and $\mathcal{F}(y) = \{1 - \exp(-y/\Lambda_I^2)\}/y$, $\Lambda_I = 1 \text{ GeV}$. We employ a mass-independent (chiral-limit) momentum-subtraction renormalisation scheme [43].

Widespread use has shown [14] that interactions in the class containing Eqs. (1), (2) can serve to unify the properties of many systems. Contemporary studies employ $\omega = 0.8 \text{ GeV}$ [44]. Then, with $\omega D = 0.8 \text{ GeV}^3$ and renormalisation point invariant quark current mass $\hat{m}_u = \hat{m}_d = 6.04 \text{ MeV}$, which corresponds to a one-loop mass at $\zeta = 2 \text{ GeV}$ of 4.19 MeV , the

following predictions are obtained: pion mass $m_\pi = 0.14 \text{ GeV}$; nucleon mass $m_N = 0.94 \text{ GeV}$; and pion leptonic decay constant $f_\pi = 0.094 \text{ GeV}$. These values align with experiment [45]. When the product ωD is kept fixed, physical observables remain practically unchanged under $\omega \rightarrow (1 \pm 0.2)\omega$ [46].

All subsequent calculations are parameter-free. The interaction involves one parameter and there is a single quark current-mass. Both quantities are now fixed.

Before continuing, it is worth providing additional context for the interaction in Eq. (2) by noting that, following Ref. [41], one may draw a connection between $\tilde{\mathcal{G}}$ and QCD’s process-independent effective charge, discussed in Refs. [47, 48]. That effective charge is characterised by an infrared coupling value $\hat{\alpha}(0)/\pi = 0.97(4)$ and a gluon mass-scale $\hat{m}_0 = 0.43(1) \text{ GeV}$ determined in a combined continuum and lattice analysis of QCD’s gauge sector [47]. The following values are those of analogous quantities inferred from Eq. (2):

$$\alpha_{\tilde{\mathcal{G}}}(0)/\pi = 1.45, \quad m_{\tilde{\mathcal{G}}} = 0.54 \text{ GeV}. \quad (3)$$

They agree tolerably with the QCD values, especially if one recalls that earlier, less well informed versions of the RL interaction yielded $\alpha_{\tilde{\mathcal{G}}}(0)/\pi \approx 15$, *i.e.*, a value ten-times larger [41].

2.2. Nucleon electromagnetic current

Working with the solution of the Faddeev equation in Fig. 2, the interaction current drawn in Fig. 3 is necessary and sufficient to deliver a photon + nucleon interaction that is consistent with all relevant Ward-Green-Takahashi identities; hence, *inter alia*, ensures electromagnetic current conservation [49, Sec. III.A]. The current can be written as follows ($N = p, n$):

$$J_\mu^N(Q) = ie\Lambda_+(p_f)[F_1^N(Q^2)\gamma_\mu + \frac{1}{2m_N}\sigma_{\mu\nu}Q_\nu F_2^N(Q^2)]\Lambda_+(p_i) \quad (4)$$

where e is the positron charge, the incoming and outgoing nucleon momenta are $p_{i,f}$, $Q = p_f - p_i$, $\Lambda_+(p_{i,f})$ are positive-energy nucleon-spinor projection operators, and $F_{1,2}^N$ are the Dirac and Pauli form factors.

The nucleon charge and magnetisation distributions are ($\tau = Q^2/[4m_N^2]$) [50]:

$$G_E^N = F_1^N - \tau F_2^N, \quad G_M^N = F_1^N + F_2^N. \quad (5)$$

Magnetic moments and radii are obtained therefrom using standard definitions: $\mu_N = G_M^N(Q^2 = 0)$;

$$\langle r_F^2 \rangle^N = -6 \frac{d \ln G_F^N(Q^2)}{dQ^2} \Big|_{Q^2=0}, \quad (6)$$

$F = E, M$, except $\langle r_E^2 \rangle^N = -6G_E^N(Q^2)|_{Q^2=0}$ because $G_E^N(0) = 0$.

Numerical methods for solving sets of coupled gap, Bethe-Salpeter, and Faddeev equations are described, *e.g.*, in Refs. [36, 37, 51, 52]. Exploiting these schemes, we solved all equations relevant to calculation of the current in Eq. (4) and computed the current itself, thereby arriving at predictions for the form factors in Eq. (5).

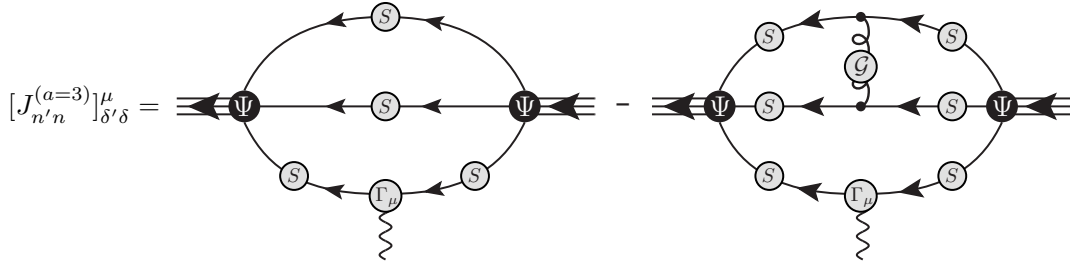


Figure 3: Since the nucleon has three valence quarks, the complete nucleon electromagnetic current has three terms: $J_\mu(Q) = \sum_{a=1,2,3} J_\mu^a(Q)$; but using symmetries, one can readily obtain the $a = 1, 2$ components once the $a = 3$ component is known [39, Appendix B]. δ, δ' are spinor indices and n, n' are isospin indices. Γ_μ is the dressed-photon+quark vertex, which can be obtained, *e.g.*, following Ref. [40].

A technical remark is appropriate here. The Faddeev equation solution depends on two relative momenta, p, q , and the nucleon total momentum, P . This leads to a dependence on three angular variables defined via the inner products $p \cdot q, p \cdot P, q \cdot P$. In solving the equation, eight Chebyshev polynomials are used to express the dependence on each angle [37]. This enables evaluation of Ψ at any required integration point in either the Faddeev equation or the current. P is a complex-valued (timelike) vector, $P^2 = -m_N^2$, whereas Q is spacelike. So, when evaluating the current, the integrand sample points are typically in the complex plane. This leads to oscillations whose amplitudes grow with Q^2 . Increasing the number of Chebyshev polynomials and quadrature points is effective on $Q^2 \lesssim 4 \text{ GeV}^2$. At larger Q^2 values, however, this brute force approach fails to deliver accurate results.

In order to obtain predictions on $Q^2 \gtrsim 4 \text{ GeV}^2$, we extrapolate using the SPM, whose properties and accuracy are explained and illustrated elsewhere – see Refs. [32–34] and citations therein and thereof. The SPM is based on the Padé approximant. It accurately reconstructs a function in the complex plane within a radius of convergence determined by that one of the function’s branch points which lies closest to the real domain that provides the sample points. Modern implementations introduce a statistical element; so, the extrapolations come with an objective and reliable estimate of uncertainty.

As noted above, numerous demonstrations of the SPM’s accuracy and reliability are available. Herein we highlight (i) that provided in connection with the proton radius puzzle [53, Supplemental Material], which shows that the SPM accurately reproduces known radii from nine distinct representations of low-energy electron + proton scattering data and (ii) an application to the search for exotic hadrons, in which the SPM was shown to reliably reproduce results obtained using five distinct models that were employed to perform a combined analysis of different partial waves in the decays $J/\psi \rightarrow \gamma\pi^0\pi^0$ and $J/\psi \rightarrow \gamma K_S^0 K_S^0$ [33, Sec. 3]. It is also worth highlighting that in these diverse applications, the SPM was applied without modification. It is a truly robust tool.

Our SPM extrapolations of the form factors onto $Q^2 \gtrsim 4 \text{ GeV}^2$ are developed as follows.

Step 1 For each function considered, we produce $N = 40$ directly calculated function values spaced evenly on $Q^2 \lesssim 4 \text{ GeV}^2$.

Table 1: Static properties: magnetic moments in nuclear magnetons and radii-squared in fm^2 , calculated using conventional definitions – Sec. 2.2. Empirical values from Ref. [45, PDG]. The column “SPM” lists radii extracted from experimental data using the SPM [32].

	herein	Exp.	SPM
μ_p	2.23	2.793	
μ_n	-1.33	-1.913	
$\langle r_E^2 \rangle^p$	0.788	0.7070(7)	0.717(14)
$\langle r_E^2 \rangle^n$	-0.0621	-0.1160(22)	
$\langle r_M^2 \rangle^p$	0.672	0.72(4)	0.667(44)
$\langle r_M^2 \rangle^n$	0.661	0.75(2)	

Step 2 From that set, $M_0 = 14$ points are chosen at random, the usual SPM continued fraction interpolation is constructed, and that function is extrapolated onto $Q^2/\text{GeV}^2 \in [4, 12]$. The curve is retained so long as it is singularity free.

Step 3 This is repeated with another set of M_0 randomly chosen points. Steps 2 and 3 admit $\approx 5 \times 10^{10}$ independent extrapolations.

Step 4 One continues with 2 and 3 until $n_{M_0} = 500$ smooth extrapolations are obtained.

Step 5 Steps 2 and 3 are repeated for $M = \{M_0 + 2i | i = 1, \dots, 6\}$

Step 6 At this point, one has 3 000 statistically independent extrapolations.

Working with these extrapolations, then at each value of Q^2 , we record the mean value of all curves as the central prediction and report as the uncertainty the function range which contains 68% of all the extrapolations – this is a 1σ band.

3. Results and Discussion

3.1. Nucleon form factors

Predictions for nucleon static (low Q^2) properties are collected in Table 1. In size, the magnetic moments are $\sim 25\%$ too small. This is a failing of RL truncation, which produces a photon+quark vertex whose dressed-quark anomalous magnetic moment term is too weak. It is corrected in higher-order

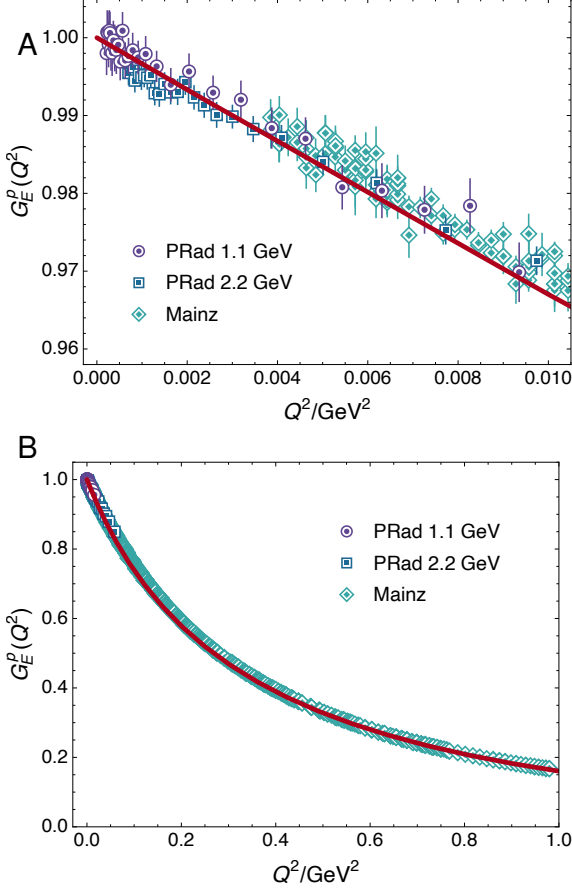


Figure 4: Low Q^2 behaviour of proton electric form factor: solid red line – result obtained herein; data from Refs. [55, Mainz] and [56, PRad].

truncations [54]. Such corrections have been implemented in studies of mesons [44]. It may be possible to adapt this approach to baryons. Concerning the other entries in Table 1, the agreement with experiment is reasonable. In particular, our analysis delivers fair agreement with extant low- Q^2 precision data on electron + proton scattering – see Fig. 4; and the prediction $\langle r_E^2 \rangle^p > \langle r_M^2 \rangle^p$ accords with SPM analyses of existing form factor measurements [32].

As displayed in Figs. 5, 6, the Faddeev equation prediction for the overall Q^2 dependence of each nucleon form factor agrees well with data [57–71]. Even $G_E^n(Q^2)$ is a fair match, despite its sensitivity to details of the neutron wave function, especially as expressed in F_1^n – see, *e.g.*, Refs. [11, 72].

It is worth quantifying the above remarks by comparing the predictions in Figs. 5, 6 with the parametrisations of data provided in Ref. [73, Kelly]. A useful measure is the relative \mathcal{L}_1 difference: $\Delta_F^N = 2[|\delta_-^N|/|\delta_+^N|]$, where

$$[\delta_{\mp}^N]_F = \int_0^{10 \text{ GeV}^2} dQ^2 \frac{|\text{Prediction}_F^N(Q^2) \mp \text{Kelly}_F^N(Q^2)|}{\text{Prediction}_F^N(Q^2)}. \quad (7)$$

The upper bound is effectively that employed in Ref. [73]. The results are:

	G_E^p	G_M^p	G_E^n	G_M^n	
$\Delta_F^N(\%)$	4.9	7.2	21	4.0	(8)

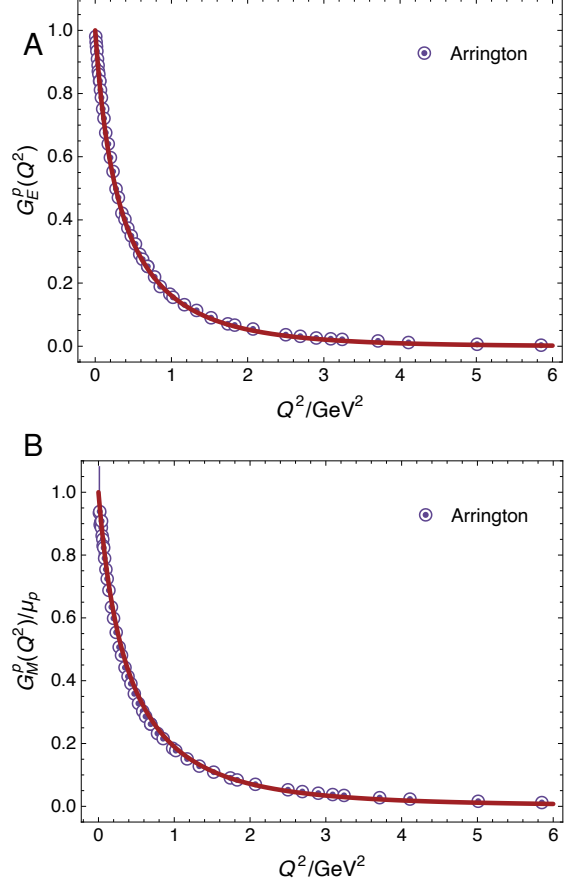


Figure 5: Proton electromagnetic form factors: solid red line – results obtained herein. Experimental data taken from compilation in Ref. [57].

Evidently, the parameter-free Faddeev equation predictions are practically indistinguishable from the data fits [73], except in the case of G_E^n , which, in the mean, lies systematically below the fit by $\approx 20\%$. These features are also illustrated in Figs. 5, 6. Regarding G_E^p , G_M^p/μ_p , G_M^n/μ_n , within line width, the data parametrisations are indistinguishable from our predictions – so, not drawn. The parametrisation is drawn in Fig. 6A, making manifest the $\approx 20\%$ underestimate of G_E^n .

3.2. Form Factor Ratios

It is appropriate here to stress that $G_M^{p,n}(Q^2)/\mu_{p,n}$ agree well with experiment. This is important in connection with the prediction for $\mu_p G_E^p(Q^2)/G_M^p(Q^2)$ drawn in Fig. 7A. Directly calculated Faddeev equation results are available on $Q^2 \lesssim 4 \text{ GeV}^2$. Thereafter, we calculate two sets of SPM results: (I) ratio formed from curves obtained via independent SPM analyses of $G_{E,M}^p$; (II) SPM analysis of the ratio $\mu_p G_E^p/G_M^p$ obtained on the directly accessible domain. Both methods yield compatible results and agree with all available data within mutual uncertainties. Significantly, a zero is predicted in G_E^p :

$$\text{SPM I: } Q_{G_E^p-\text{zero}}^2 = 8.37_{-0.81}^{+1.68} \text{ GeV}^2, \quad (9a)$$

$$\text{SPM II: } Q_{G_E^p-\text{zero}}^2 = 9.59_{-0.85}^{+2.09} \text{ GeV}^2. \quad (9b)$$

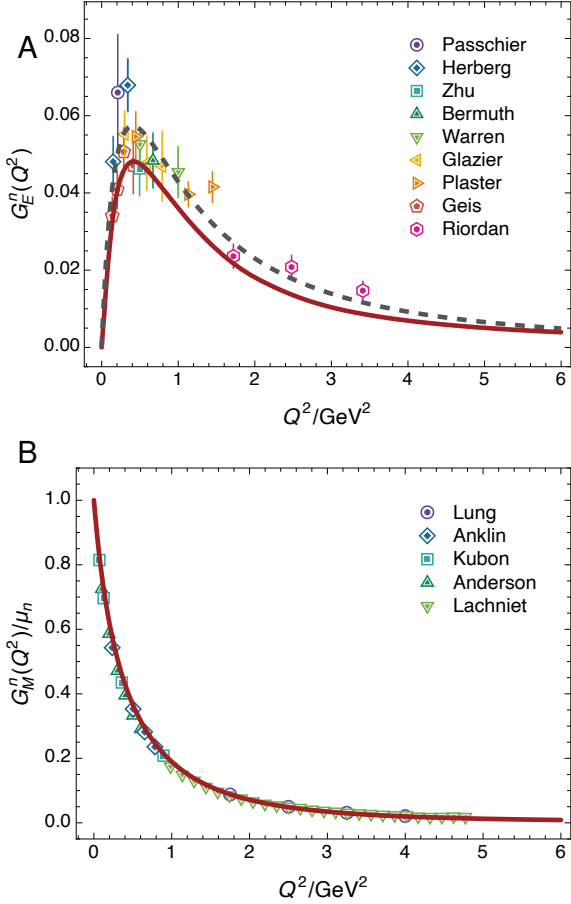


Figure 6: Neutron electromagnetic form factors. Solid red curve – results obtained herein. Dashed black curve in panel A – Ref. [73, Kelly] parametrisation of data. G_E^n experimental data: Refs. [58–66]. G_M^n data: Refs. [67–71]

Being compatible, they can be averaged, with the result:

$$Q_{G_E^n}^2 = 8.86_{-0.86}^{+1.93} \text{ GeV}^2. \quad (10)$$

Notably, we have verified the suggestion made elsewhere [74] that if the quark + quark interaction is modified such that dressed quarks more rapidly become parton like, then $Q_{G_E^n}^2$ is shifted to a larger value. The location of the zero in G_E^n is thus confirmed to be a sensitive expression of gauge sector dynamics and emergent hadron mass [13–15].

We depict the Faddeev equation prediction for $\mu_n G_E^n(Q^2)/G_M^n(Q^2)$ in Fig. 7B. The agreement with data is fair and the trend is correct. Given that our prediction delivers a good description of $G_M^n(Q^2)/\mu_n$, the quantitative mismatch owes to the imperfect description of G_E^n that was described above. No signal is found for a zero in $\mu_n G_E^n(Q^2)/G_M^n(Q^2)$. It follows that there is a Q^2 domain upon which the charge form factor of the neutral neutron is larger than that of the positively charged proton. It begins at $Q^2 = 4.66_{-0.13}^{+0.18} \text{ GeV}^2$.

At first glance, the absence of a zero in $\mu_n G_E^n(Q^2)/G_M^n(Q^2)$ conflicts with the other existing Poincaré-invariant study of nucleon form factors at large Q^2 , which employs a quark+diqark approach [76]. However, that study locates the zero at $Q_{G_E^n}^2 = 20.1_{-3.5}^{+10.6} \text{ GeV}^2$, *i.e.*, an uncertain location beyond

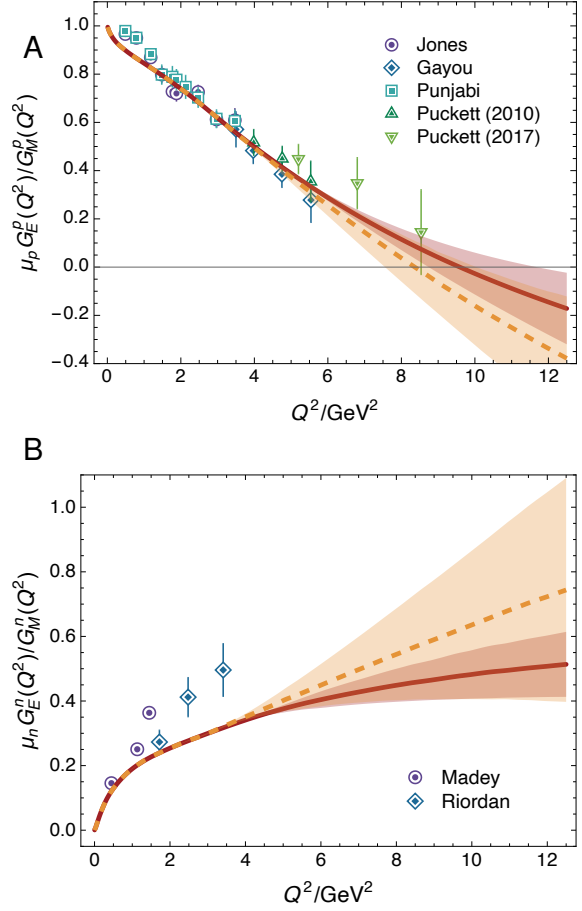


Figure 7: Panel A: $\mu_p G_E^p/G_M^p$. Panel B: $\mu_n G_E^n/G_M^n$. SPM I – dashed orange curve within like-coloured band; and SPM II – solid red curve within like-coloured band. Data: proton – Refs. [18–22]; and neutron – Refs. [66, 75].

the range of foreseeable measurements.

Naturally, given the simplicity of the quark + diqark approach, some differences should be expected between our predictions and the results in Ref. [76]. Comparisons are nevertheless worthwhile because they can inform the improvement of both approaches. Indeed, given that its simplicity enables straightforward application to a wide range of problems, the value of a refined quark + diqark approach should not be underestimated. It is important, therefore, to observe that the predictions herein and those in Ref. [76] are largely in semiquantitative agreement, even though apparently minor differences are amplified at large Q^2 . This means that an efficacious refinement of the quark + diqark picture is achievable.

3.3. Flavour Separation

Supposing one can neglect strange quark contributions to nucleon form factors, which is a good approximation [77], then a flavour separation is possible using the following identities:

$$F_i^u = 2F_i^p + F_i^n, \quad F_i^d = F_i^p + 2F_i^n, \quad i = 1, 2. \quad (11)$$

Current conservation and valence-quark number entail $F_1^u(Q^2 = 0) = 2$, $F_1^d(Q^2 = 0) = 1$.

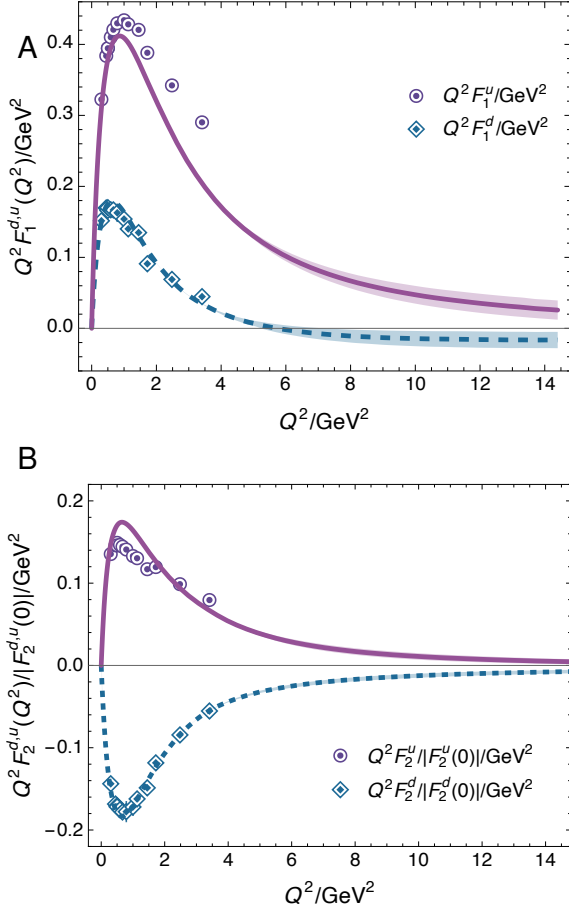


Figure 8: Flavour separation of proton form factors: $Q^2 F_1^{d,u}(Q^2)$ (Panel A); and $Q^2 F_2^{d,u}(Q^2)/F_2^{d,u}(0)$ (Panel B). Data: Ref. [23].

Our parameter-free predictions for these form factors are drawn in Fig. 8. They deliver good agreement with available data. *N.B.* To account for the RL truncation underestimate of nucleon magnetic moments, the Pauli form factors in Fig. 8B – both experiment and theory – are normalised by the magnitude of their $Q^2 = 0$ values. Regarding Fig. 8A, it is worth highlighting that the apparent mismatch between our prediction for F_1^u and larger Q^2 data is somewhat misleading owing to amplification via Q^2 multiplication. On the displayed domain, the true relative \mathcal{L}_1 difference between prediction and data is just 6%. There is room for improvement in the RL treatment of the three-valence-body problem, but it does provide a reliable foundation. Notably, a zero is projected in F_1^d at

$$Q_{F_1^d\text{-zero}}^2 = 5.73_{-0.49}^{+1.46} \text{ GeV}^2. \quad (12)$$

This matches the result obtained in the quark+diuark picture [76]: $Q^2 = 7.0_{-0.4}^{+1.1} \text{ GeV}^2$.

No signal is found for a zero in any other form factor in Fig. 8. The quark + diuark picture produces an uncertain zero in F_2^d at very large momentum transfer: $Q^2 = 12.0_{-1.7}^{+3.9} \text{ GeV}^2$.

As explained elsewhere [72], in the isospin symmetry limit, the behaviours of $\mu_p G_E^p(Q^2)/G_M^p(Q^2)$ and $\mu_n G_E^n(Q^2)/G_M^n(Q^2)$ are not independent. This is readily seen by exploiting isospin

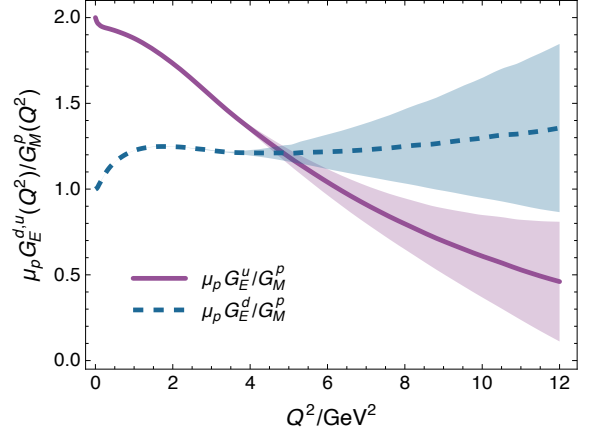


Figure 9: Flavour separation of the charge and magnetisation form factors, with each function normalised by G_M^p in order to highlight their differing Q^2 -dependence.

symmetry in writing a flavour separation of the charge and magnetisation form factors ($e_u = 2/3$, $e_d = -1/3$):

$$G_E^p = e_u G_E^{pu} + e_d G_E^{pd}, \quad G_E^n = e_u G_E^{pn} + e_d G_E^{pn}. \quad (13)$$

Regarding these identities, we refer to Fig. 9 and note that G_E^p possesses a zero because, although remaining positive, G_E^{pu}/G_M^p falls steadily with increasing Q^2 whereas G_E^{pd}/G_M^p is positive and approximately constant. On the other hand and consequently, G_E^n does not exhibit a zero because $e_u > 0$, G_E^{pn}/G_M^p is large and positive, and $|e_d G_E^{pn}|$ is always less than $e_u G_E^{pn}$.

The character of G_E^{pd}/G_M^p owes to the fact that F_2^d is negative definite on the entire domain displayed in Fig. 8 – because F_2^n is negative thereupon, see Eq. (11) – and $G_E^d = F_1^d - (Q^2/[4m_N^2])F_2^d$, whereas F_1^d falls toward its zero from above.. This is not the case for the quark + diuark calculation, in which F_2^d also exhibits a zero; so, at some Q^2 , G_E^{pd} begins to diminish in magnitude – see, e.g., Ref. [78, Fig. 7.3]. Plainly, the larger Q^2 behaviour of F_2^d is key to the existence/absence of a zero in G_E^n .

Notwithstanding these differences, it is clear that, as in the quark + diuark picture [76], if the zero in G_E^p/G_M^p moves to larger Q^2 , then G_E^n/G_M^n exhibits slower growth on $Q^2 \gtrsim Q_{F_1^d\text{-zero}}^2$. This correlation is also consistent with results obtained using IQCD [79].

Somewhat parenthetically, it is interesting to observe that, using the meson bound-state analogue of the approach employed herein [40], both the charged ρ - and K^* -meson electric form factors are predicted to exhibit a zero, whereas no zero is predicted in the neutral- K^* form factor. The explanation for the absence of a zero in the neutral- K^* electric form factor [40] is similar to that presented for G_E^n . Notably, relocating the zero in G_E^p by the ratio m_p^2/m_ρ^2 , it is placed at $9.4(3) \text{ GeV}^2$, within the domain defined by Eqs. (9). Furthermore, the electric form factor of the $J = 1$ deuteron also exhibits a zero [80]. These remarks highlight that it is perhaps typical for the electric form factor of an electrically charged $J \neq 0$ bound state to possess a zero, owing to the potential for destructive interference be-

tween the leading charge form factor and magnetic and higher multipole form factors – see, *e.g.*, Eq. (5). This is not the case for $J = 0$ [81] because such systems have only one electromagnetic form factor, $F_{J=0}$, and both valence contributions to $F_{J=0}$ are alike in sign.

4. Summary and Perspectives

Using a symmetry-preserving truncation of the quantum field equations relevant to calculation of hadron masses and interactions, this study delivers parameter-free predictions for all nucleon charge and magnetisation distributions and their flavour separation. Each element in this analysis possesses an unambiguous link with analogous quantities in quantum chromodynamics (QCD) and the study unifies nucleon properties with those of numerous other hadrons – see, *e.g.*, Refs. [14, 81, 82]. These features provide support for the reliability of the results herein.

The proton electric form factor, $G_E^p(Q^2)$, is predicted to possess a zero at a Q^2 location within reach of modern experiments [Fig. 7A and Eq. (10)]. On the other hand, the neutron electric form factor, G_E^n , does not exhibit a zero [Fig. 7B]. Consequently, anticipated experiments will see $|G_E^n/G_E^p| > 1$, *i.e.*, an electric form factor of the charge-neutral neutron that is greater than that of the charge-one proton. As revealed by a form factor flavour separation, these outcomes rest with the behaviour of the proton’s d -quark Pauli form factor [Sec. 3.3]. Each of the highlighted form factor features are sensitive expressions of emergent phenomena in QCD.

No material improvement of the analysis herein can be anticipated before a way is found to include higher-order truncations in the continuum baryon bound-state problem or lattice-regularised QCD produces precise results on a similar domain to that discussed herein. Meanwhile, the framework used herein can be applied to other high-profile challenges [2–7], *e.g.*, prediction of baryon electroweak form factors, nucleon-to-resonance transition form factors, and nucleon gravitational form factors. Such studies are underway.

Declaration of competing interest — The authors declare that they have no known competing financial interests or personal relationships that could have appeared to influence the work reported in this paper.

Data availability — This manuscript has no associated data or the data will not be deposited. [Authors’ comment: All information necessary to reproduce the results described herein is contained in the material presented above.]

Acknowledgments — We are grateful for constructive interactions with P. Cheng, L. Liu, S.-X. Qin and Z.-N. Xu. Work supported by: National Natural Science Foundation of China (grant no. 12135007); Natural Science Foundation of Jiangsu Province (grant no. BK20220122); and STRONG-2020 “The strong interaction at the frontier of knowledge: fundamental research and applications” which received funding from the European Union’s Horizon 2020 research and innovation programme (grant agreement no. 824093).

References

- [1] W. J. Marciano, H. Pagels, Quantum Chromodynamics: A Review, *Phys. Rept.* 36 (1978) 137.
- [2] M. Ablikim, M. N. Achasov, P. Adlarson, et al. (BESIII), Future Physics Programme of BESIII, *Chin. Phys. C* 44 (2020) 040001.
- [3] D. P. Anderle, V. Bertone, X. Cao, et al., Electron-ion collider in China, *Front. Phys. (Beijing)* 16 (2021) 64701.
- [4] R. Abdul Khalek, A. Accardi, J. Adam, et al., Science Requirements and Detector Concepts for the Electron-Ion Collider: EIC Yellow Report, *Nucl. Phys. A* 1026 (2022) 122447.
- [5] C. Quintans, The New AMBER Experiment at the CERN SPS, *Few Body Syst.* 63 (2022) 72.
- [6] D. S. Carman, R. W. Gothe, V. I. Mokeev, C. D. Roberts, Nucleon Resonance Electroexcitation Amplitudes and Emergent Hadron Mass, *Particles* 6 (2023) 416–439.
- [7] V. I. Mokeev, P. Achenbach, V. D. Burkert, D. S. Carman, R. W. Gothe, A. N. Hiller Blin, E. L. Isupov, K. Joo, K. Neupane, A. Trivedi, First Results on Nucleon Resonance Electroexcitation Amplitudes from $ep \rightarrow e'\pi^+\pi^-p'$ Cross Sections at $W = 1.4$ - 1.7 GeV and $Q^2 = 2.0$ - 5.0 GeV², *Phys. Rev. C* 108 (2023) 025204.
- [8] R. F. Streater, A. S. Wightman, PCT, Spin and Statistics, and All That, 3rd ed., Addison-Wesley, Reading, Mass, 1980.
- [9] J. Glimm, A. Jaffe, Quantum Physics. A Functional Point of View, Springer-Verlag, New York, 1981.
- [10] Y. Aoki, T. Blum, G. Colangelo, et al. (Flavour Lattice Averaging Group (FLAG)), FLAG Review 2021, *Eur. Phys. J. C* 82 (2022) 869.
- [11] G. Eichmann, H. Sanchis-Alepuz, R. Williams, R. Alkofer, C. S. Fischer, Baryons as relativistic three-quark bound states, *Prog. Part. Nucl. Phys.* 91 (2016) 1–100.
- [12] V. D. Burkert, C. D. Roberts, Colloquium: Roper resonance: Toward a solution to the fifty-year puzzle, *Rev. Mod. Phys.* 91 (2019) 011003.
- [13] D. Binosi, Emergent Hadron Mass in Strong Dynamics, *Few Body Syst.* 63 (2022) 42.
- [14] M. Ding, C. D. Roberts, S. M. Schmidt, Emergence of Hadron Mass and Structure, *Particles* 6 (2023) 57–120.
- [15] M. N. Ferreira, J. Papavassiliou, Gauge Sector Dynamics in QCD, *Particles* 6 (2023) 312–363.
- [16] M. Y. Barabanov, M. A. Bedolla, W. K. Brooks, et al., Diquark Correlations in Hadron Physics: Origin, Impact and Evidence, *Prog. Part. Nucl. Phys.* 116 (2021) 103835.
- [17] G. Eichmann, R. Alkofer, A. Krassnigg, D. Niemorus, Nucleon mass from a covariant three-quark Faddeev equation, *Phys. Rev. Lett.* 104 (2010) 201601.
- [18] M. K. Jones, K. A. Aniol, F. T. Baker, et al., G_{E_p}/G_{M_p} ratio by polarization transfer in $\vec{e}p \rightarrow e\vec{p}$, *Phys. Rev. Lett.* 84 (2000) 1398–1402.
- [19] O. Gayou, K. A. Aniol, T. Averett, et al., Measurement of $G(E_p)/G(M_p)$ in $\vec{e}p \rightarrow e\vec{p}$ to $Q^2 = 5.6$ GeV², *Phys. Rev. Lett.* 88 (2002) 092301.
- [20] V. Punjabi, C. F. Perdrisat, K. A. Aniol, et al., Proton elastic form factor ratios to $Q^2 = 3.5$ GeV² by polarization transfer, *Phys. Rev. C* 71 (2005) 055202. [Erratum-ibid. **C71**, 069902 (2005)].
- [21] A. J. R. Puckett, E. J. Brash, M. K. Jones, et al., Recoil Polarization Measurements of the Proton Electromagnetic Form Factor Ratio to $Q^2 = 8.5$ GeV², *Phys. Rev. Lett.* 104 (2010) 242301.
- [22] A. J. R. Puckett, E. J. Brash, M. K. Jones, et al., Polarization Transfer Observables in Elastic Electron Proton Scattering at $Q^2 = 2.5, 5.2, 6.8,$ and 8.5 GeV², *Phys. Rev. C* 96 (2017) 055203. [erratum: *Phys. Rev. C* **98**, 019907 (2018)].
- [23] G. Cates, C. de Jager, S. Riordan, B. Wojtsekhowski, Flavor decomposition of the elastic nucleon electromagnetic form factors, *Phys. Rev. Lett.* 106 (2011) 252003.
- [24] B. Wojtsekhowski, Flavor Decomposition of Nucleon Form Factors – arXiv:2001.02190 [nucl-ex], 2020.
- [25] C. F. Perdrisat, V. Punjabi, M. Vanderhaeghen, Nucleon electromagnetic form factors, *Prog. Part. Nucl. Phys.* 59 (2007) 694–764.
- [26] G. A. Miller, Transverse Charge Densities, *Ann. Rev. Nucl. Part. Sci.* 60 (2010) 1–25.
- [27] R. Holt, R. Gilman, Transition between nuclear and quark-gluon descriptions of hadrons and light nuclei, *Rept. Prog. Phys.* 75 (2012) 086301.
- [28] V. Punjabi, C. F. Perdrisat, M. K. Jones, E. J. Brash, C. E. Carlson, The

- Structure of the Nucleon: Elastic Electromagnetic Form Factors, *Eur. Phys. J. A* 51 (2015) 79.
- [29] S. J. Brodsky, V. D. Burkert, D. S. Carman, et al., Strong QCD from Hadron Structure Experiments, *Int. J. Mod. Phys. E* 29 (2020) 2030006.
- [30] G. Gilfoyle, Future Measurements of the Nucleon Elastic Electromagnetic Form Factors at Jefferson Lab, *EPJ Web Conf.* 172 (2018) 02004.
- [31] D. Binosi, L. Chang, S.-X. Qin, J. Papavassiliou, C. D. Roberts, Symmetry preserving truncations of the gap and Bethe-Salpeter equations, *Phys. Rev. D* 93 (2016) 096010.
- [32] Z.-F. Cui, D. Binosi, C. D. Roberts, S. M. Schmidt, Hadron and light nucleus radii from electron scattering, *Chin. Phys. C* 46 (2022) 122001.
- [33] D. Binosi, A. Pilloni, R.-A. Tripolt, Study for a model-independent pole determination of overlapping resonances, *Phys. Lett. B* 839 (2023) 137809.
- [34] Z.-F. Cui, D. Binosi, C. D. Roberts, S. M. Schmidt, D. N. Triantafyllopoulos, Fresh look at experimental evidence for odderon exchange, *Phys. Lett. B* 839 (2023) 137826.
- [35] Q.-W. Wang, S.-X. Qin, C. D. Roberts, S. M. Schmidt, Proton tensor charges from a Poincaré-covariant Faddeev equation, *Phys. Rev. D* 98 (2018) 054019.
- [36] S.-X. Qin, C. D. Roberts, S. M. Schmidt, Poincaré-covariant analysis of heavy-quark baryons, *Phys. Rev. D* 97 (2018) 114017.
- [37] P. Maris, C. D. Roberts, π and K meson Bethe-Salpeter amplitudes, *Phys. Rev. C* 56 (1997) 3369–3383.
- [38] A. Bashir, A. Raya, S. Sánchez-Madriral, C. D. Roberts, Gauge invariance of a critical number of flavours in QED3, *Few Body Syst.* 46 (2009) 229–237.
- [39] G. Eichmann, C. S. Fischer, Nucleon axial and pseudoscalar form factors from the covariant Faddeev equation, *Eur. Phys. J. A* 48 (2012) 9.
- [40] Y.-Z. Xu, D. Binosi, Z.-F. Cui, B.-L. Li, C. D. Roberts, S.-S. Xu, H.-S. Zong, Elastic electromagnetic form factors of vector mesons, *Phys. Rev. D* 100 (2019) 114038.
- [41] S.-X. Qin, L. Chang, Y.-X. Liu, C. D. Roberts, D. J. Wilson, Interaction model for the gap equation, *Phys. Rev. C* 84 (2011) 042202(R).
- [42] D. Binosi, L. Chang, J. Papavassiliou, C. D. Roberts, Bridging a gap between continuum-QCD and *ab initio* predictions of hadron observables, *Phys. Lett. B* 742 (2015) 183–188.
- [43] L. Chang, Y.-X. Liu, C. D. Roberts, Y.-M. Shi, W.-M. Sun, H.-S. Zong, Chiral susceptibility and the scalar Ward identity, *Phys. Rev. C* 79 (2009) 035209.
- [44] Z.-N. Xu, Z.-Q. Yao, S.-X. Qin, Z.-F. Cui, C. D. Roberts, Bethe-Salpeter kernel and properties of strange-quark mesons, *Eur. Phys. J. A* 59 (2023) 39.
- [45] S. Navas, C. Amsler, T. Gutsche, et al., Review of particle physics, *Phys. Rev. D* 110 (2024) 030001.
- [46] S.-X. Qin, C. D. Roberts, Impressions of the Continuum Bound State Problem in QCD, *Chin. Phys. Lett.* 37 (2020) 121201.
- [47] Z.-F. Cui, J.-L. Zhang, D. Binosi, F. de Soto, C. Mezrag, J. Papavassiliou, C. D. Roberts, J. Rodríguez-Quintero, J. Segovia, S. Zafeiropoulos, Effective charge from lattice QCD, *Chin. Phys. C* 44 (2020) 083102.
- [48] S. J. Brodsky, A. Deur, C. D. Roberts, The Secret to the Strongest Force in the Universe, *Sci. Am.* 5 (May) (2024) 32–39.
- [49] G. Eichmann, Nucleon electromagnetic form factors from the covariant Faddeev equation, *Phys. Rev. D* 84 (2011) 014014.
- [50] R. Sachs, High-Energy Behavior of Nucleon Electromagnetic Form Factors, *Phys. Rev.* 126 (1962) 2256–2260.
- [51] P. Maris, P. C. Tandy, QCD modeling of hadron physics, *Nucl. Phys. Proc. Suppl.* 161 (2006) 136–152.
- [52] A. Krassnigg, Excited mesons in a Bethe-Salpeter approach, *PoS CONFINEMENT 8* (2008) 075.
- [53] Z.-F. Cui, D. Binosi, C. D. Roberts, S. M. Schmidt, Fresh extraction of the proton charge radius from electron scattering, *Phys. Rev. Lett.* 127 (2021) 092001.
- [54] L. Chang, Y.-X. Liu, C. D. Roberts, Dressed-quark anomalous magnetic moments, *Phys. Rev. Lett.* 106 (2011) 072001.
- [55] J. C. Bernauer, P. Achenbach, C. Ayerbe Gayoso, et al., High-precision determination of the electric and magnetic form factors of the proton, *Phys. Rev. Lett.* 105 (2010) 242001.
- [56] W. Xiong, A. Gasparian, H. Gao, et al., A small proton charge radius from an electron-proton scattering experiment, *Nature* 575 (2019) 147–150.
- [57] J. Arrington, W. Melnitchouk, J. A. Tjon, Global analysis of proton elastic form factor data with two-photon exchange corrections, *Phys. Rev. C* 76 (2007) 035205.
- [58] I. Passchier, R. Alarcon, T. S. Bauer, et al., The Charge form-factor of the neutron from the reaction ${}^2\text{H}(\vec{e}, e'n)p$, *Phys. Rev. Lett.* 82 (1999) 4988–4991.
- [59] C. Herberg, M. Ostrick, H. G. Andresen, et al., Determination of the neutron electric form-factor in the $\text{D}(e, e'n)p$ reaction and the influence of nuclear binding, *Eur. Phys. J. A* 5 (1999) 131–135.
- [60] H. Zhu, A. Ahmidouch, H. Anklin, et al. (E93026), A Measurement of the electric form-factor of the neutron through $\vec{d}(\vec{e}, e'n)p$ at $Q^2 = 0.5 (\text{GeV}/c)^2$, *Phys. Rev. Lett.* 87 (2001) 081801.
- [61] J. Bermuth, P. Merle, C. Carasco, et al., The Neutron charge form-factor and target analyzing powers from ${}^3\text{He}(\vec{e}, e'n)$ scattering, *Phys. Lett. B* 564 (2003) 199–204.
- [62] G. Warren, F. R. Wesselmann, H. Zhu, et al., Measurement of the electric form-factor of the neutron at $Q^2 = 0.5$ and $1.0 \text{ GeV}^2/c^2$, *Phys. Rev. Lett.* 92 (2004) 042301.
- [63] D. Glazier, M. Seimetz, J. R. M. Annand, et al., Measurement of the electric form-factor of the neutron at $Q^2 = 0.3 (\text{GeV}/c)^2$ to $0.8 (\text{GeV}/c)^2$, *Eur. Phys. J. A* 24 (2005) 101–109.
- [64] B. Plaster, A. m. Semenov, A. Aghalaryan, et al., Measurements of the neutron electric to magnetic form-factor ratio G_E^n/G_M^n via the ${}^2\text{H}(\vec{e}, e'\vec{n})\text{H}$ reaction to $Q^2 = 1.45 (\text{GeV}/c)^2$, *Phys. Rev. C* 73 (2006) 025205.
- [65] E. Geis, M. Kohl, V. Ziskin, et al. (BLAST), The Charge Form Factor of the Neutron at Low Momentum Transfer from the ${}^2\text{H}(\vec{e}, e'n)p$ Reaction, *Phys. Rev. Lett.* 101 (2008) 042501.
- [66] S. Riordan, S. Abrahamyan, B. Craver, A. Kelleher, A. Kolarkar, et al., Measurements of the Electric Form Factor of the Neutron up to $Q^2 = 3.4 \text{ GeV}^2$ using the Reaction ${}^3\text{He}(\vec{e}, e'n)pp$, *Phys. Rev. Lett.* 105 (2010) 262302.
- [67] A. Lung, L. M. Stuart, P. E. Bosted, et al., Measurements of the electric and magnetic form-factors of the neutron from $Q^2 = 1.75 (\text{GeV}/c)^2$ to $4 (\text{GeV}/c)^2$, *Phys. Rev. Lett.* 70 (1993) 718–721.
- [68] H. Anklin, L. J. deBever, K. I. Blomqvist, et al., Precise measurements of the neutron magnetic form-factor, *Phys. Lett. B* 428 (1998) 248–253.
- [69] G. Kubon, H. Anklin, P. Bartsch, et al., Precise neutron magnetic form-factors, *Phys. Lett. B* 524 (2002) 26–32.
- [70] B. Anderson, T. Auerbach, L. Annd Averett, et al. (Jefferson Lab E95-001), Extraction of the Neutron Magnetic Form Factor from Quasi-elastic ${}^3\text{He}(\vec{e}, e')$ at $Q^2 = 0.1 - 0.6 (\text{GeV}/c)^2$, *Phys. Rev. C* 75 (2007) 034003.
- [71] J. Lachniet, A. Afanasev, H. Arenhovel, et al. (CLAS), A Precise Measurement of the Neutron Magnetic Form Factor G_M^n in the few- GeV^2 Region, *Phys. Rev. Lett.* 102 (2009) 192001.
- [72] J. Segovia, I. C. Cloet, C. D. Roberts, S. M. Schmidt, Nucleon and Δ elastic and transition form factors, *Few Body Syst.* 55 (2014) 1185–1222.
- [73] J. J. Kelly, Simple parametrization of nucleon form factors, *Phys. Rev. C* 70 (2004) 068202.
- [74] I. C. Cloet, C. D. Roberts, A. W. Thomas, Revealing dressed-quarks via the proton's charge distribution, *Phys. Rev. Lett.* 111 (2013) 101803.
- [75] R. Madey, A. Y. Semenov, S. Taylor, et al., Measurements of G_E^n/G_M^n from the ${}^2\text{H}(\vec{e}, e'\vec{n})$ reaction to $Q^2 = 1.45 (\text{GeV}/c)^2$, *Phys. Rev. Lett.* 91 (2003) 122002.
- [76] Z.-F. Cui, C. Chen, D. Binosi, F. de Soto, C. D. Roberts, J. Rodríguez-Quintero, S. M. Schmidt, J. Segovia, Nucleon elastic form factors at accessible large spacelike momenta, *Phys. Rev. D* 102 (2020) 014043.
- [77] P. E. Shanahan, R. Horsley, Y. Nakamura, D. Pleiter, P. E. L. Rakow, G. Schierholz, H. Stüben, A. W. Thomas, R. D. Young, J. M. Zanotti, Determination of the strange nucleon form factors, *Phys. Rev. Lett.* 114 (2015) 091802.
- [78] I. C. Cloet, C. D. Roberts, Explanation and Prediction of Observables using Continuum Strong QCD, *Prog. Part. Nucl. Phys.* 77 (2014) 1–69.
- [79] C. Kallidonis, S. Syritsyn, M. Engelhardt, J. Green, S. Meinel, J. Negele, A. Pochinsky, Nucleon electromagnetic form factors at high Q^2 from Wilson-clover fermions, *PoS LATTICE2018* (2018) 125.
- [80] M. Kohl, Elastic form factors of the proton, neutron and deuteron, *Nucl. Phys. A* 805 (2008) 361–368.
- [81] Z.-Q. Yao, D. Binosi, C. D. Roberts, Onset of scaling violation in pion and kaon elastic electromagnetic form factors, *Phys. Lett. B* 855 (2024) 138823.
- [82] G. Eichmann, C. S. Fischer, W. Heupel, N. Santowsky, P. C. Wallbott,

Four-quark states from functional methods, *Few Body Syst.* 61 (2020)
38.